LAWRENCE
LIVERMORE
NATIONAL
LABORATORY

UCRL-JRNL-203456

Hydrogen Sensor Based on Yttria-Stabilized Zirconia Electrolyte and Tin-Doped Indium Oxide Sensing Electrode

L. P. Martin, R. S. Glass

April 9, 2004

Journal of the Electrochemical Society

Hydrogen Sensor Based on Yttria-Stabilized Zirconia Electrolyte and Tin-Doped Indium Oxide Sensing Electrode

L. Peter Martin* and Robert. S. Glass

Lawrence Livermore National Laboratory, Mail code: L-353

P.O. Box 808, Livermore, CA 94551

*Corresponding author: Phone: 925-423-9831, Fax: 925-423-7040, email: martin89@llnl.gov

ABSTRACT

A solid state electrochemical sensor has been developed for hydrogen leak detection in ambient air. The sensor uses an yttria-stabilized electrolyte with a tin-doped indium oxide sensing electrode and a Pt reference electrode. Excellent sensitivity, and response time of one second or less, are reported for hydrogen gas over the concentration range of 0.03 to 5.5% in air. Cross-sensitivity to relative humidity and to CO_2 are shown to be low. The response to methane, a potentially significant source of interference for such a sensor, is significantly less than that for hydrogen. The sensor shows good reproducibility and was unaffected by thermal cycling over the course of this investigation. The effects of sensing electrode thickness and thermal aging are also reported, and the sensing mechanism is discussed. The sensor is intended for use in vehicles powered by hydrogen fuel cells and hydrogen internal combustion engines. Those vehicles will use and/or store significant quantities of hydrogen, and will require safety sensor for monitoring potential hydrogen leakage in order to ensure passenger safety.

PACS codes: 82.47.Rs, 07.07.Df

Keywords: Hydrogen, fuel cell vehicles, sensor, potentiometric, ITO, yttria-stabilized zirconia

INTRODUCTION

Proton exchange membrane (PEM) fuel cells being developed for fuel cell vehicles require the use of a high hydrogen concentration fuel stream. The hydrogen can be generated on-board using a fuel (e.g., natural gas) reformer or supplied from an on-board storage system. At present, the automobile manufacturers are concentrating most of their efforts on systems that store hydrogen on-board, and this is currently thought to be the most probable method to be commercialized in the near future. In order to reach acceptable driving range requirements, 4-5 kg of hydrogen must be stored on board the vehicle. On-board storage systems under development include gas or liquid phase storage in pressurized (ambient temperature or cryogenic) tanks, and solid state storage in metal hydrides, carbon materials, or chemical hydrides. Current prototype vehicles use compressed-gas tank storage systems, and it seems likely that this storage method will be the earliest to be widely deployed. In these compressed-gas tanks hydrogen is typically stored at 5,000-10,000 psi. [1]

Hydrogen is a colorless, odorless gas which, when mixed with air, is flammable in the 4-75%% (by volume) concentration range. Furthermore, hydrogen oxidation flames cannot be seen in direct sunlight. For these reasons, the potential accumulation of hydrogen in or around hydrogen-powered vehicles must be monitored to ensure passenger safety. The most significant potential sources of hydrogen leakage are from mechanical failure of storage tanks, shut off/isolation valves, pressure relief devices, pressure regulation valves, and piping and fittings. Catastrophic failure of the tank is considered unlikely, particularly while the vehicle is parked. Failure of the pressure relief device, though unlikely, is most probable during refueling. The highest risk areas for leakage are the valves, piping and fittings. As a result, general concerns over passenger safety will require placement of hydrogen sensors at strategic locations under a

vehicle and in the passenger cabin. A detection threshold of 1% and response time on the order of 1 s have been identified as adequate sensor performance targets.[2] The 1% detection threshold is analogous to codes for natural gas use in vehicle parking structures, where United States National Fire Protection Agency Code 497 mandates sensors for detection at 25% of the lower flammability limit.

A number of sensors for hydrogen detection have been investigated for various different applications. These include sensors based on: thermoelectric effect [3], fiber optic/surface plasmon [4], solid state electrochemical [5, 6, 7], MOS devices [8], surface acoustic wave [9], and others [10-15]. At present, none of these sensors have been demonstrated to have the aggregate characteristics desired by the automobile and fuel cell manufacturers. Particularly problematic are the requirements for response time (1 second or less) and resistance to humidity (10 to 100% relative humidity). To illustrate this point, Table I lists various hydrogen sensor technologies, and approximate response times as reported in the literature. This Table is by no means an exhaustive survey of the literature, and comparison of these sensor responses is somewhat unfair due to the wide variety of test conditions cited in these various references. However, the point that can be drawn from this Table, and from other sources, is that the target response time of 1 s or less required for automotive safety applications is by no means trivial for any of these sensor technologies.

Currently the only gas sensor to be widely used on commercial automobiles is the exhaust gas oxygen (EGO) sensor which was introduced in response to increasing emission standards in the 1960's and 1970's. The EGO sensor is a solid state, potentiometric, electrochemical sensor that uses a yttria-stabilized zirconia electrolyte. It is used in the exhaust stream of internal combustion engines to control the air/fuel stoichiometry and minimize

emission of hydrocarbons, NO_x and CO. This sensor meets the rigid requirements for use on-board automobiles and has established solid state electrochemical sensors using yttria-stabilized zirconia electrolytes as viable candidates for automotive gas sensing in general.

We have developed a solid state electrochemical sensor for hydrogen leak detection. The intended application for this sensor is to detect hydrogen, at <1% concentration in ambient air, in order to provide for an adequate safety system for PEM fuel cell vehicles using on-board hydrogen storage. The sensor uses a yttria-stabilized zirconia electrolyte with a tin-doped indium (ITO) sensing electrode and Pt reference electrode. Non-equilibrium red-ox potentials are generated on the sensing and reference electrodes, and the difference between these electrode potentials is measured and correlated to the hydrogen concentration in the range of ~0.02 – 5.5%. The measured response time is less than 1 s for hydrogen concentrations greater than 0.03% in air. The sensor shows good selectivity to hydrogen and is not responsive to H_2O and CO_2 over the ranges tested. The response to methane is significantly less than that for hydrogen. In the work reported here, the sensor was tested at 450-550^oC in a laboratory tube furnace to insure adequate ionic conductivity in the (relatively) thick electrolyte. For a deployable safety sensor, the device could be fabricated on an RTD heated substrate in thin film form and encased in a protective (antistatic, antispark) housing. The power requirements to heat the thin film to a localized surface temperature of 500^oC should be in the mW range, fitting well with automotive sensor goals.

EXPERIMENTAL

Sensors were fabricated by attaching porous electrodes to dense yttria-stabilized zirconia (YSZ) electrolyte substrates. The YSZ substrates were prepared from a commercial powder

(Tosoh 8YS) by tape casting and sintering in air at 1550 ^{o}C for three hours. The final thickness of the substrates was 200 μm, and examination using scanning electron microscopy showed high density with minimal, isolated pores. On each electrolyte, a sensing electrode was applied by colloidal spray deposition of a commercially available, nanocrystalline Sn-doped In_2O_3 powder (Nanophase, NanoTek ITO-0600). The In/Sn ratio is 9/1, and the average particle size is specified by the manufacturer as 21 nm. To reduce particle agglomeration from the as-received state, the powder was milled in ethanol for 48 hours. To perform the spray deposition, the powder was dispersed in an ethanol/water solution and sprayed onto the dense YSZ substrate using an ultrasonic nozzle.[16] Multiple passes were required to deposit coatings of appropriate thickness to perform as sensor electrodes. A reference electrode was applied to each sensor on the opposite face from the ITO electrode by painting on a commercial Pt ink (Englehard, 6082). The ITO and Pt electrodes were co-sintered in air at 900^{o}C.

H_2 sensing experiments were performed by exposing the sensor to flowing gas inside a quartz reaction tube (inside diameter of 15.88 mm) placed inside a tube furnace. The entire metal-oxide/YSZ/metal sensor is exposed to the test gas (i.e. no reference gas is used). Pt wires were used to connect the external leads to the sensor electrodes. Light pressure was used to insure good contact between the Pt wires and the sensing and reference electrodes. All tests were performed by mixing dry and humidified air with H_2, CO_2 or CH_4 at a flow rate of 1000 ml/min. Test temperatures ranged from 450 to 550^{o}C. A standard gas handling system was used to deliver the gasses to the reaction tube. The open circuit potential of the sensors was recorded using an electrochemical interface (Radiometer Analytical, Voltalab PGZ301). Measured potentials represent the difference in electrode potential at the sensing (ITO) and reference (Pt) electrodes with both electrodes exposed to the test gas.

RESULTS AND DISCUSSION

Operating Principal - The sensor response is defined as the open circuit potential measured between the ITO sensing electrode and the Pt reference electrode. The potential at each electrode is determined by the kinetic balance of all the electrochemical reactions occurring on the electrode (sometimes called a 'mixed potential'). In the presence of hydrogen and air, the generally accepted sensing mechanism at the electrodes in an electrochemical cell of this type is associated with the simultaneous, competing oxidation-reduction reactions [5]:

$$1/2O_2 + 2e^- \leftrightarrow O^{2-} \quad (1)$$

$$H_2 + O^{2-} \leftrightarrow H_2O + 2e^- \quad (2)$$

where O^{2-} represents an oxide ion supplied by the YSZ lattice and the other terms have their usual meanings. Under these conditions, a local cell supporting both reaction is created at each electrode, and the overall sensor response is related to the difference in the individual electrode potentials caused by the different reaction rates on the two different electrode materials.

For a single electrode, reactions (1) and (2) will each have an associated local current density, i_{O_2} and i_{H_2}, respectively. The steady state electrode potential, E_{SS}, is uniquely defined by the condition that the total electrode current is zero:

$$i_{H_2} + i_{O_2} = 0 \quad (3)$$

By making the appropriate substitutions for i_{H_2} and i_{O_2} from the Butler-Volmer equation, the steady state electrode potential can be shown to be logarithmically dependent upon both the H_2 and O_2 concentrations [5, 17]

$$E_{SS} = A_1 + A_2 \ln[C(O_2)] - A_3 \ln[C(H_2)] \quad (4)$$

where A_1, A_2, and A_3 are constants which account for the catalytic activity of the electrode

materials through their dependence on the charge transfer coefficients, and the standard rate constants associated with the exchange current densities. Analogous equations can be written for both the sensing, E_{SS}^{Sense}, and reference, E_{SS}^{Ref} electrodes. The measured sensor response, E_m, is the difference between the respective steady state potential at the two electrodes,

$$E_m = E_{SS}^{Sense} - E_{SS}^{Ref} = C_1 + C_2\, ln[C(O_2)] - C_3\, ln[C(H_2)] \qquad (5)$$

where C_1, C_2, and C_3 are constants incorporating the constant terms from Eq. (4) for each of the two electrodes. Similar discussion involving metal oxide sensing electrode response has been made for stabilized-zirconia-based NO_x [18, 19], H_2S [20], and CO [17, 21, 22] sensors. Because the changes in $C(O_2)$ are due to dilution of the oxygen by the addition of hydrogen, $C(O_2)$ is related to $C(H_2)$ by:

$$C(O_2) = 0.21\{1 - C(H_2)\} \qquad (6)$$

where 0.21 is the fraction of O_2 in ambient air. Eq. (6) simply states that the test gas is composed of air and hydrogen, and that the air must be 21% oxygen. As a result, Eq. (5) becomes

$$E_m = C_1 + C_2\, ln[0.21(1 - C(H_2))] - C_3\, ln[C(H_2)] \qquad (7)$$

This treatment obviously neglects any direct, gas-phase reaction of O_2 and H_2 to form H_2O, e.g. Eq. (8) below, which could potentially shift the O_2/H_2 ratio since it consumes twice as many hydrogen molecules as oxygen per formula unit. However, it will be shown below that this expression, Eq. (7), accurately describes the observed sensor response over a wide range of test conditions.

Sensing electrode thickness - The effect of sensing electrode thickness on sensor response was evaluated by fabricating a series of sensors with thicknesses ranging from 2 to 13

μm. Sensitivity to H_2 was tested at 500°C in flowing air at 10% relative humidity. In all cases the reference electrodes were 2.5 - 3.5 μm thick, the variation resulting from the manual application of the Pt ink. Sensor response is shown in Figure 1a as a function of hydrogen concentration for each sensing electrode thickness. The data were acquired shortly after reaching the test temperature, and so represent the initial, un-aged condition of the sensors. The sensor response is nearly linear with the log of the H_2 concentration up to ~2%, where the sensitivity begins to decline slightly. It will be shown below that this reduced sensitivity at high H_2 concentration is a result of the dilution of the O_2 concentration caused by the H_2 addition to the test gas. The negative sign of the sensor response is consistent with the oxidation of H_2 at the sensing electrode being the 'dominant' reaction in determining the sensor potential, which will also be discussed below. At 1% H_2 concentration the absolute value sensor response is ~250-300 mV, depending upon sensing electrode thickness. The thickness of the sensing electrode has a clear effect on the sensor response at all H_2 concentrations, with thicker electrodes exhibiting a lower response. This implies that the charge transfer reactions responsible for the sensing response do not happen uniformly through the thickness of the electrode, but are concentrated at or near the electrolyte. The decrease in response noted upon increasing electrode thickness can thus be explained by considering that the surface of the ITO can catalyze the gas-phase reaction of H_2 and O_2:

$$H_2 + \tfrac{1}{2}\, O_2 = H_2O \qquad \Delta G(500^oC) = -28.8 \text{ kJ/mol} \tag{8}$$

The reaction shown in Eq. (8) does not involve charge transfer with the electrolyte, and thus does not contribute to the electrochemical response. Consumption of H_2 by Eq. (8) at the external surfaces of the ITO electrode will deplete the amount of hydrogen available for the charge transfer reaction at the interior of the electrode. Thicker electrodes have longer diffusion paths

for H_2 in the pores, and more surface area on which the recombination reaction can take place. Thus, less H_2 will reach the sensing region of the electrode than in thinner electrodes, and the sensor will exhibit a concurrently reduced sensing response as shown in Fig. 1a. A similar effect has been reported in stabilized zirconia-based potentiometric NO sensors.[23]

During testing at 500°C, some sensor aging effects were noted. In an attempt to accelerate the aging process, the samples were aged in air for 24 hours at 600°C and then re-tested at 500°C. The results are shown in Figure 1b, where the sensors exhibit qualitatively the same response-behavior as prior to aging, but with increased sensitivity at all H_2 concentrations. Additional aging of selected sensors at 500°C for 60 hours showed no further change in the sensitivity. At present, the source of the performance improvement during the early part of the aging process is unclear. It is tempting to attribute the aging to microstructural coarsening of either or both of the electrodes. However, the microstructures appear to be stable at 500°C, and do not exhibit any significant coarsening even after many days at the operating temperature. Figure 2 shows the ITO electrode microstructure before and after aging in air at 600°C for 24 hours followed by 500°C for 260 hours. The initial microstructure (Fig. 2a) is very fine, with particle sizes ranging from 30 to 100 nm. As can be seen, after aging (Fig. 2b), there is no discernable change the ITO microstructure. Similarly, Figure 3 shows the microstructure of the Pt reference material before and after the same thermal aging. While the Pt microstructure is significantly coarser than the ITO electrode, it also shows no significant coarsening during the aging process. The difference in the thickness between the Pt layers in Figures 3a and 3b results from variations in the manual application of the ink used to fabricate the electrode.

Also shown in Figure 1a and 1b are curves generated from non-linear regression fitting of Eq. (7) to the experimental data. These data demonstrate that the sensor response to H_2 is well

described by Eq. (7). Upon inspection of Eq. (7), it is clear that for constant $C(O_2)$ the expected sensor response is linear with the logarithm of the H_2 concentration, $C(H_2)$. That scenario clearly does not describe the sensor response at high $C(H_2)$. It is only by allowing $C(O_2)$ to decrease with increasing $C(H_2)$, as described by Eq. (6), that Eq. (7) can describe the sensor response over the range of $C(H_2)$ tested here. Thus, the decreased sensor response at the highest H_2 concentrations, in Figs. 1a and b, is a predictable consequence of the dilution of O_2 resulting from the addition of H_2 to the test gas.

Table II shows the parameters C_1, C_2, and C_3 used to generate the curves to fit Eq. (7) to the aged-sensor data in Figure 1b. It is interesting to note the sign of the C_2 and C_3 terms in Table II. For a single electrode, the form of Eq. (4) requires the sign of the A_2 and A_3 terms to both be the same. This ensures that the oxygen reduction, Eq. (1), and the hydrogen oxidation, Eq. (2), reactions shift the electrode potential in opposite directions, as they must by definition. Also, it is observed experimentally, using a concentration cell with the reference electrode exposed to ambient air, that both of these electrode materials (ITO and Pt) shift the cell potential in the same direction: negative or positive when exposed to increasing or decreasing $C(H_2)$, respectively.[24] This means that not only must the A_2 and A_3 terms have the same sign on each electrode, but that all four of these terms (A_2^{Sense}, A_2^{Ref}, A_3^{Sense}, A_3^{Ref}) must have the same sign. This fact allows interpretation of the fitting parameters from Table II. From Eqs. (4) and (5)

$$C_2 = A_2^{Sense} - A_2^{Ref} \tag{9}$$

$$C_3 = A_3^{Sense} - A_3^{Ref} \tag{10}$$

Thus, in Table II, the negative sign for C_2 indicates that $A_2^{Sense} < A_2^{Ref}$, while the positive sign for C_3 indicates that $A_3^{Sense} > A_3^{Ref}$. This implies that, under these test conditions, the reference electrode dominates the overall sensor response with respect to the oxygen reaction, Eq. (1)

above, while the sensing electrode dominates the sensor response with respect to the hydrogen reaction, Eq. (2). The significance is that, by proper selection of a reference electrode material with a less favorable O_2 response, the possibility exists to design a sensor which suppresses the observed reduction in response at high $C(H_2)$.

As with other reported sensors of this type, sensor response is observed to decrease with increasing temperature due to the enhancement of reaction kinetics.[5, 18, 23] Figure 4 shows the dependence of the H_2 response on furnace temperature for an aged sensor with a 13 μm sensing electrode. At 550°C, the data exhibit qualitatively similar behavior to that seen in Fig. 1b, but with reduced sensitivity. Upon reducing the temperature to 500°C, the sensor demonstrates the expected temperature-related increase in sensor response at all H_2 concentrations. When the temperature is further reduced to 450°C, the sensitivity enhancement is smaller and decays with increasing H_2 concentration until the data converge with the 500°C data. This convergence was also exhibited by other sensors with different ITO thicknesses. This behavior is probably related to either: a) the competing response of the Pt reference electrode, which increases rapidly as the temperature decreases, or b) the inability of the entire system to reach the same quasi-equilibrium steady state as at higher temperature due in general to the reduced reaction kinetics, and in particular to the reduced oxide ion conductivity in the YSZ. Figure 4 also shows curve fitting of Eq. (7) to the data. The sensor response is well described by Eq. (7) over the temperature range from 450 - 550°C.

It was observed that sensor baselines were significantly affected by both thickness and aging of the sensing electrode. Sensor baseline is defined as the open circuit voltage measured between the sensing and reference electrodes in ambient air, i.e. in the absence of H_2. Sensors with thicker sensing electrodes consistently tend to achieve baselines in the absence of H_2 (open

circuit potential in air) which are closer to zero. This implies that the thicker electrodes tend to exhibit oxygen reaction (Eq. (2) above) kinetics which are more similar to the Pt reference electrodes. This effect is shown in Figure 5, where sensor baselines in ambient air are shown as a function of operating temperature for three sensors with sensing electrode thickness 2, 8 and 13 microns. All three electrodes were aged at 600^{o}C in air for 24 hours. The sensor baselines become more negative with decreasing sensing electrode thickness and operating temperature. In addition, it was observed that the sensor baselines drift during the initial aging process. Upon initial testing, all sensors started out with baselines near zero at all test temperatures >450 ^{o}C. After aging, sensors with thinner electrodes equilibrate at the non-zero baselines shown in Figure 5. This is shown in Table III, where the baseline at 500^{o}C is given for the same three sensors before and after the 600^{o}C, 24 hour aging treatment. The baselines stabilize during this aging treatment, and further aging does not significantly affect the measured baselines. The exact mechanism determining the baselines, and their evolution during aging is not clear at present. While it is likely related to microstructural aging, precise determination is complicated by the fact that the measured response is a superposition of the combined responses of the two (sensing and reference) electrodes. Thus, aging processes at both electrodes must be considered. Investigation of these effects are currently underway.

Cross-sensitivity - Based on the tradeoff between sensitivity, baseline values, aging, and operating temperature, sensor parameters were selected for further characterization and testing. An operating temperature of 500^{o}C was selected to maximize sensitivity and baseline stability for the sensing electrode thickness of ~13 micron. Further evaluation is categorized into: cross-sensitivity, response time, and long-term stability. Figure 6 shows the H_2 response at 500^{o}C in 10% and 90% relative humidity. The sensor, with a 13 μm sensing electrode, was aged in air for

over 100 hours at 500°C prior to acquisition of these data. Each pair of curves represents a measurement before and after 18 hrs at 90% relative humidity. The test sequence progressed as follows. H_2 response data were taken after a long isothermal dwell (100 hours) at 10% relative humidity in air (solid triangles in Fig. 6). The relative humidity was adjusted to 90%, and H_2 sensitivity data were acquired again after approximately 10 minutes (open diamonds). After 18 hours at 90% relative humidity, H_2 response data were acquired again (open triangles). Finally, the relative humidity was adjusted back to 10%, and the sensor response was re-tested again (solid triangles). These data indicate that the sensor is fairly insensitive to relative humidity in the 10-90% range., with a change in response of not more than 10% (in the positive direction) in going from 10% to 90%. In addition, the sensor response is stable and reproducible over this same humidity range over the duration of the test.

Figure 6 also shows the sensor response to CH_4, H_2O, and CO_2 over varying concentration ranges. The indicated CO_2 concentrations represent the excess above the ambient air level (~1%) It can be seen that the sensor is not responsive to H_2O and CO_2 over the ranges tested. In contrast, the sensor responds to CH_4 , although with a significantly lower response than to H_2.

Response time - Sensor response versus time, acquired at a 0.01-s sampling rate, is shown in Figure 7a for 0.03, 0.12, 0.67, and 2.7% H_2 in air with10% relative humidity. It is interesting to note that the sensor response exhibits an 'overshoot' which increases in magnitude as the H_2 concentration increases. This behavior can be caused by pressure transients associated with the gas handling system. However, extensive experiments performed under a variety of different gas handling configurations confirmed that this effect is, for the present sensor, not an

artifact of pressure or flow-rate transients. Rather, the effect seems to be related to the interfering effect of H_2 sensitivity at the reference electrode. Recall that, for this sensor, both electrodes are exposed to the test gas. From a practical standpoint, this is a desirable configuration because it avoids the added complexity of providing an isolated reference electrode exposed to a reference gas. Of course, any sensitivity to the gas under test at the reference electrode will shift the reference point against which the response of the sensing electrode is being measured. In our case, ITO and Pt, the potential response resulting from introduction of H_2 is in the same direction (negative). Because the two electrodes respond similarly, the net effect is that the Pt response reduces the magnitude of the overall sensor response. The data shown in Figure 7a are consistent with a scenario in which the reference electrode is both less sensitive and slower responding than the sensing electrode. Thus, upon introduction of H_2 the sensor exhibits a rapid response corresponding to the response characteristics of the sensing electrode. As the slower reference electrode begins to respond, the potential difference between the sensing and reference electrode declines to a smaller absolute magnitude, eventually reaching a stable level equal to the difference between the individual electrode responses. This behavior was observed to evolve as a function of sensor aging. Initially, and up to approximately 80 hours of aging at 500^{o}C, the sensor response did not exhibit the overshoot transient to any significant degree. This can be seen in Figure 7b, where the temporal response of the sensor to 0.5% H_2 in air is shown after 86, 117, 124, and 148 hours of operation. At 86 hours, the overshoot is just beginning to manifest. It becomes more apparent with additional aging. It is interesting to note that the steady state response of the sensor does not change significantly during this part of the aging process. This indicates that, if the transient overshoot signal is solely determined by the reference electrode, the aging process is affecting the response time but not the overall response

amplitude of the Pt electrode.

Returning to Figure 7a, response times were measured for different H_2 concentrations on the transient generated upon introduction of hydrogen, taking into account the ultimate final potential reached after the "overshoot." For example, in Figure 7a the response time for 2.7% hydrogen was determined in relation to the point 'a' on the transient. Response times were calculated from the baseline to 90% of full response (t_{90}) and from 10% to 90% of the full response ($t_{10\text{-}90}$). The latter value is probably somewhat more accurate in that there is a noise-limited error involved in identifying the point at which the sensor response deviates from the baseline. The resultant data are shown in Figure 8, where the t_{90} and $t_{10\text{-}90}$ response times are shown as a function of H_2 concentration. Based on these data, response times decrease with increasing H_2 concentration and are less than 1 s for concentrations greater than 0.03%. This is completely acceptable for a hydrogen sensor to be used in safety applications for hydrogen leaks on vehicles. [2]

Long-term testing - Figure 9 shows the effect of aging on sensor response to 0.3% H_2 in air. The response data are plotted versus the aging time, t, at i) 600^{o}C (t = 0 - 24 hrs), then ii) 500^{o}C (t > 24 hrs). The first response datum at time t = 0 represents the initial (un-aged) sensor response measured at 500^{o}C. The second point at t = 24 hours represents the response, measured at 500^{o}C, after 24 hours at 600^{o}C. All subsequent measurements show the sensor response after additional time at 500^{o}C. Also shown in the Figure is the sensor baseline, in the absence of H_2, prior to the response measurements. During the first 150 hours of this test, the sensor was cooled to room temperature repeatedly (6 times) for durations ranging from 18 hours to two weeks. The data shown in the figure corresponds to the actual time at 500^{o}C, irrespective of temperature

cycling. As seen in Figure 9, the response and baseline are quite stable over the duration of the test, 250±10 mV and 12±10 mV, respectively. These data demonstrate that the sensor sensitivity and reproducibility are not affected by thermal cycling.

CONCLUSIONS

We report a solid state electrochemical sensor for detecting up to ~5% hydrogen in ambient air. Potential applications involve safety and leak detection on-board hydrogen fuel cell or hydrogen fueled internal combustion engine vehicles. The sensor uses an yttria-stabilized zirconia electrolyte with an ITO sensing electrode and Pt reference electrode. The hydrogen concentration, in air, is correlated with the open circuit potential measured between the electrodes. The sensor exhibits pseudo-logarithmic response to hydrogen over the concentration range of 0.03 to 2.5%, with a decrease in response at higher concentrations due to the associated dilution of O_2 in the air. It was found that, over the temperature range of 450-550^{o}C, increased temperature reduces the sensor response. The sensor was nearly insensitive to relative humidity in the 10-90% range, and showed no response to CO_2 . The response to hydrogen was significantly larger than that for methane, ranging from 6/1 at 0.02% to 1.7/1 at 2.5%. The measured response times were 1 s or less at hydrogen concentrations from 0.03% to 5.5%. The sensor showed good reproducibility and appeared to be unaffected by thermal cycling.

Sensors with different sensing electrode thickness in the range of 2-13 μm were investigated. It was found that thicker ITO electrodes show decreased response to hydrogen. This is thought to be due to the increased contribution of hydrogen/oxygen recombination, which dilutes the effective hydrogen concentration reaching the sensing region of the electrode. Finally sensor aging effects were explored. It was found that initial aging of the sensors at 600^{o}C in air

for 24 hr resulted in improved sensor response, with additional aging not resulting in further improvement. The reason for this is not clear; however, since no noticeable microstructural changes were observed during aging.

The measured sensitivity and response time for the sensor fits in well with automobile manufacturer goals. In addition, the desired detection level of 1% in air (25% of the lower flammability limit) is well with the response range of the sensor. We note that in the work reported here, the sensor was tested inside a tube furnace to insure adequate control of the temperature. For a deployable safety sensor, the device could be fabricated on an RTD-heated substrate in thin film form and encased in a protective (antistatic, antispark) housing. In that form, the power requirements to heat the thin film to the operating temperature are anticipated to be in the 100-500 mW range.

ACKNOWLEDGEMNTS

This work was performed under the auspices of the U. S. Department of Energy by the University of California, Lawrence Livermore National Laboratory under Contract No. W-7405-Eng-48.

References

1. "National Hydrogen Energy Roadmap," U. S. Department of Energy, November 2002.

2. *Sensor needs and Requirements for Proton-Exchange Membrane Fuel Cell Systems and Direct-Injection Engines*, R.S. Glass, J. Milliken, K. Howden, and R Sullivan, eds., (Lawrence Livermore National Laboratory, UCRL-ID-137767, Livermore, CA, 2000) pp. 11-12.

3. M. Matsumiya, O. Fabin, W. Shin, N. Izu, N. Murayama, S. Kanzaki, "Thin-film Li-doped NiO for thermoelectric hydrogen gas sensor," *Thin Solid Films*, **419** [1-2] 213-17 (2002).

4. X. Bevenot, A. Trouillet, C. Veillas, H. Gagnaire, M. Clement, "Surface plasmon resonance hydrogen sensor using an optical fibre," *Measurement Science & Technology*, **13** [1] 118-24 (2002).

5. G. Lu, N. Miura, and N. Yamazoe, "High-temperature hydrogen sensor based on stabilized zirconia and a metal oxide electrode," *Sensors and Actuators B*, **35** [1-3] 130-135 (1996).

6. K. Katahira, H. Matsumoto, H. Iwahara, K. Koide, T. Iwamoto, "A solid electrolyte hydrogen sensor with an electrochemically-supplied hydrogen standard," *Sensors & Actuators B*, **73** [2-3] 130-4 (2001).

7. Y.-C. Liu, B.-J. Hwang, and I.-J. Tzeng, "Solid-State Amperometric Hydrogen Sensor Using Pt/C/Nafion Composite Electrodes Prepared by a Hot-Pressed Method," *J. Electrochem. Soc.*, **149**, [11] H173-178 (2002).

8. D. Dwivedi, R. Dwivedi, S.K. Srivastava, "Sensing properties of palladium-gate MOS (Pd-MOS) hydrogen sensor-based on plasma grown silicon dioxide," *Sensors & Actuators B*, **71** [3] 161-8 (2000).

9. W.P. Jakubik, M.W. Urbaficzyk, S. Kochowski, J. Bodzenta, "Bilayer structure for hydrogen detection in a surface acoustic wave sensor system," *Sensors & Actuators B*, **82** [2-3] 265-71

(2002).

10. D.R. Baselt, B. Fruhberger, E. Klaassen, S. Cemalovic, C.L. Britton Jr., S.V Patel, T.E. Mlsna, D. McCorkle, B. Warmack, "Design and performance of a microcantilever-based hydrogen sensor," *Sensors & Actuators B*, **88** [2] 120-31 (2003).

11. W.-C. Liu, K.-W. Lin, H.-I. Chen, C.-K. Wang, C.-C. Cheng, S.-Y. Cheng, C.-T. Lu, "A new Pt/oxide/$In_{0.49}Ga_{0.51}P$ MOS Schottky diode hydrogen sensor," *IEEE Electron Device Letters*, **23** [11] 640-2 (2002).

12. M. Radecka, K. Zakrzewska, and M. Rekas, "SnO_2-TiO_2 solid solutions for gas sensors," *Sensors & Actuators B*, **47** [1-3] 194-204 (1998).

13. N.J. Dayan, S.R. Sainkar, R.N. Karekar, and A.C. Aiyer, "A thick-film hydrogen sensor based on a ZnO:MoO_3 formulation," *Meas. Sci. and Tech.*, **9** 360-64 (1998).

14. F.-C. Lin, Y. Takao, Y. Shimizu, and M. Egashira, "Hydrogen-sensing mechanism of zinc oxide varistor gas sensors," *Sensors & Actuators B*, **24-25** 843-50 (1995).

15. G. Kaltenpoth, P. Schnabel, E. Menke, E.C. Walter, M. Grunze, and R. M. Penner, "Multimode Detection of Hydrogen Gas Using Palladium-Covered Silicon μ-Channels," *Anal. Chem.*, **75** 4756-65 (2003).

16. Pham A.-Q., Lee T. H., Glass R. S., Solid Oxide Fuel Cells (SOFC VI), *Proceedings of the Sixth International Symposium* (Electrochem. Soc., Pennington, NJ, 1999) pp.172-8.

17. C.O. Park, S.A. Akbar, W. Weppner, "Ceramic Electrolytes and Electrochemical Sensors," *J. Mat. Sci.*, **38** 4639-60 (2003).

18. G. Lu, N. Miura, and N. Yamazoe, "High-temperature sensors for NO and NO_2 based on stabilized zirconia and spinel-type oxide electrodes," *J. Mat. Chem.*, **7** 1445-49 (1997).

19. H. Kurosawa, Y. Yan, N. Miura, and N. Yamazoe, "Stabilized zirconia-based NO_x sensor

operative at high temperature," *Solid State Ionics*, **79** 338-43 (1995).

20. N. Miura, Y. Yan, G. Lu, and N. Yamazoe, "Sensing characteristics and mechanism of hydrogen sulfide sensor using stabilized zirconia and oxide sensing electrode," *Sensors & Actuators B*, **34** [1-3] 367-72 (1996).

21. Z.Y. Can, H. Narita, J. Mizusaki, and H. Tagawa, "Detection of carbon monoxide by using zirconia oxygen sensor," *Solid State Ionics*, **79** 344-48 (1995).

22. N. Miura, T. Raisen, G. Lu, and N. Yamazoe, "Highly selective CO sensor using stabilized zirconia and a couple of oxide electrodes," *Sensors & Actuators B*, **47** 84-91 (1998).

23. L.P. Martin, A.-Q. Pham, and R. S. Glass, "Effect of Cr2O3 electrode morphology on the nitric oxide response of a stabilized zirconia sensor," *Sensors & Actuators B*, **96** 53-60 (2003).

24. L.P. Martin, unpublished work.

Figure captions

Figure 1a: Initial sensor response at 500°C as a function of H_2 concentration for sensors with sensing electrode thickness of 2, 8, and 13 μm. The dotted lines show the best fit of Eq. (7) to the data.

Figure 1b: Sensor response to H_2 concentration at 500°C after aging for 24 hours at 600°C. Data are shown for the same sensors as Figure 3a, with sensing electrodes of 2, 8, and 13 μm. The dotted lines show the best fit of Eq. (7) to the data.

Figure 2: SEM micrograph of ITO electrodes: a) prior to aging, and b) after aging for 24 hours at 600°C, then 260 hours at 500°C.

Figure 3: SEM micrograph of Pt electrodes: a) prior to aging, and b) after aging for 24 hours at 600°C, then 260 hours at 500°C.

Fig 4: Sensor response (13 μm sensing electrode) versus H_2 concentration at 450, 500 and 550°C. The dotted lines show the best fit of Eq. (7) to the data.

Figure 5: Baselines in ambient air versus operating temperature for aged sensors with sensing electrode thicknesses of 2, 8, and 13 μm.

Figure 6: Response at 500°C of an aged sensor (13 μm sensing electrode) to H_2 in 10% (♦, ▲) and 90% (◊, Δ) relative humidity (RH). The two curves at each humidity level represent before and after 18 hrs at 90% relative humidity (see text). Also shown, response to CH_4, CO_2, and H_2O.

Figure 7a: Sensor response at 500°C versus time for 2.7, 0.67, 0.12 and 0.03% H_2.

Figure 7b: Evolution of the transient overshoot in the sensor response to 0.5% H_2 after operation at 500°C for: a) 86 hrs, b) 117 hrs, c) 124 hrs, and d) 148 hrs.

Figure 8: Sensor response time as a function of H_2 concentration. Response times are measured from the baseline to 90% of the full response (t_{90}) and from 10% to 90% of the full response ($t_{10\text{-}90}$).

Figure 9: Sensor baseline (●) and response to 0.3% H_2 (♦) as a function of time at 500°C.

Table I: Various types of hydrogen sensor reported in the literature, and their related response times.

Table II: Fitting parameters C_1, C_2 and C_3 used to fit Eq. (7) to the data from Figure 1b showing the response of aged sensors tested at 500°C.

Table III. Steady-state baseline at 500°C for the same three sensors as Figure 5 both before and after the 600°C, 24 hour aging treatment.

Table I: Various types of hydrogen sensor reported in the literature, and their related response times.

Technology	Reference	Response time [s]
Thermoelectric	3	50-100
Optical fiber/surface plasmon	4	3 - 300
Electrochemical (ZnO)	5	5-10
Electrochemical - active H_2 standard	6	10-100
Amperometric (nafion)	7	50-300
MOS (Pd-MOS)	8	10-25
Surface acoustic wave	9	100 - 1000
Micro-cantilever	10	90
Schottky diode	11	>1

Table II: Fitting parameters C_1, C_2 and C_3 used to fit Eq. (7) to the data from Figure 1b. Note that these parameters were calculated in units of volts using volume-fraction for the gas concentrations. These were converted to units of mV and %, respectively, to generate the curves in Figure 1b.

Thickness [μm]	C_1 [V]	C_2 [V]	C_3 [V]
2	-2.41	-1.20	0.033
8	-2.78	-1.44	0.036
13	-2.99	-1.60	0.040

Table III. Steady-state baseline at 500°C for the same three sensors as Figure 5 both before and after the 600°C, 24 hour aging treatment.

Baseline at 500°C		
WE thickness [micron]	Initial [mV]	Aged [mV]
2	-18	-43
8	-4	-22
13	-1	-7

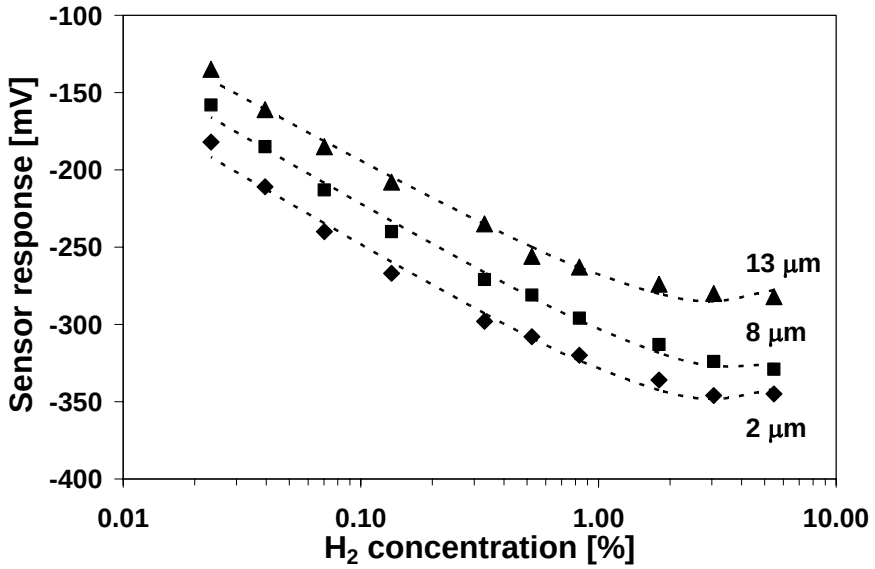

Figure 1a: Initial sensor response at 500°C as a function of H_2 concentration for sensors with sensing electrode thickness of 2, 8, and 13 μm. The dotted lines show the best fit of Eq. (7) to the data.

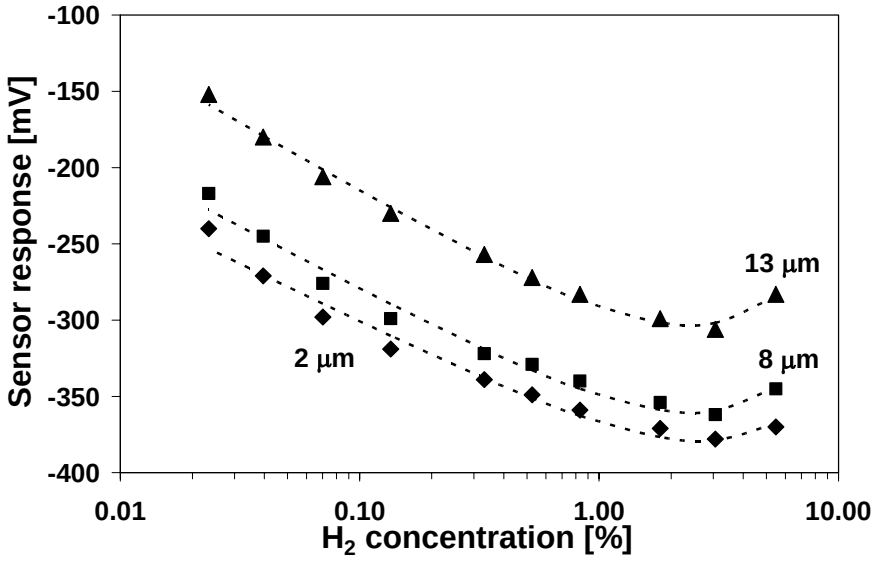

Figure 1b: Sensor response to H_2 concentration at 500°C after aging for 24 hours at 600°C. Data are shown for the same sensors as Figure 3a, with sensing electrodes of 2, 8, and 13 μm. The dotted lines show the best fit of Eq. (7) to the data.

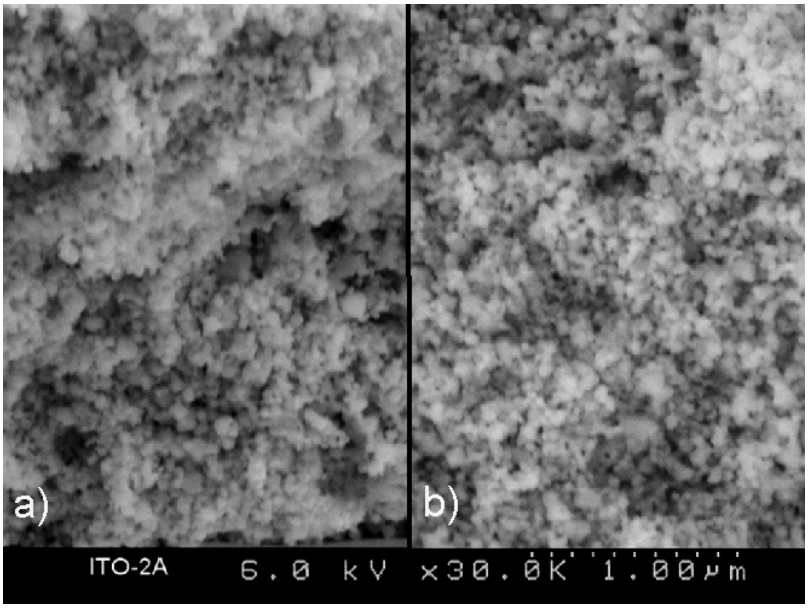

Figure 2: SEM micrograph of ITO electrodes: a) prior to aging, and b) after aging for 24 hours at 600°C, then 260 hours at 500°C.

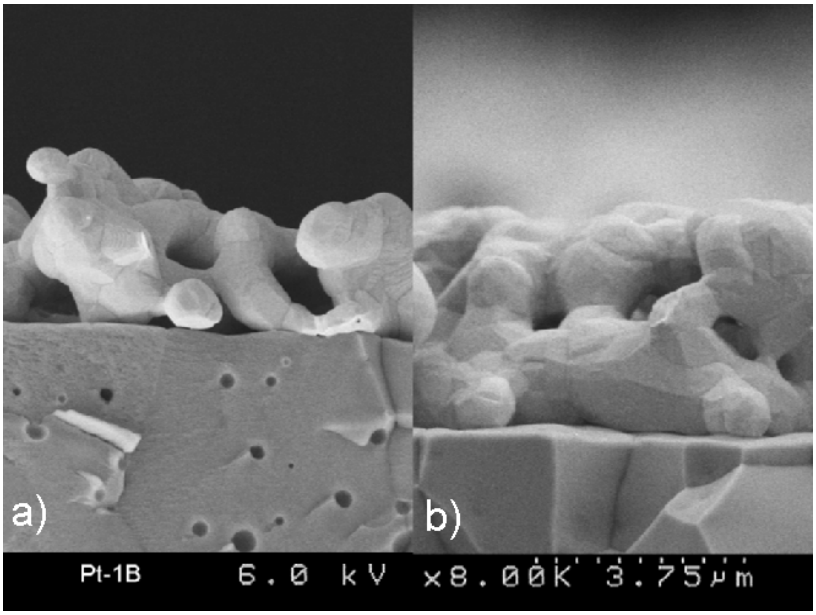

Figure 3: SEM micrograph of Pt electrodes: a) prior to aging, and b) after aging for 24 hours at 600ºC, then 260 hours at 500ºC.

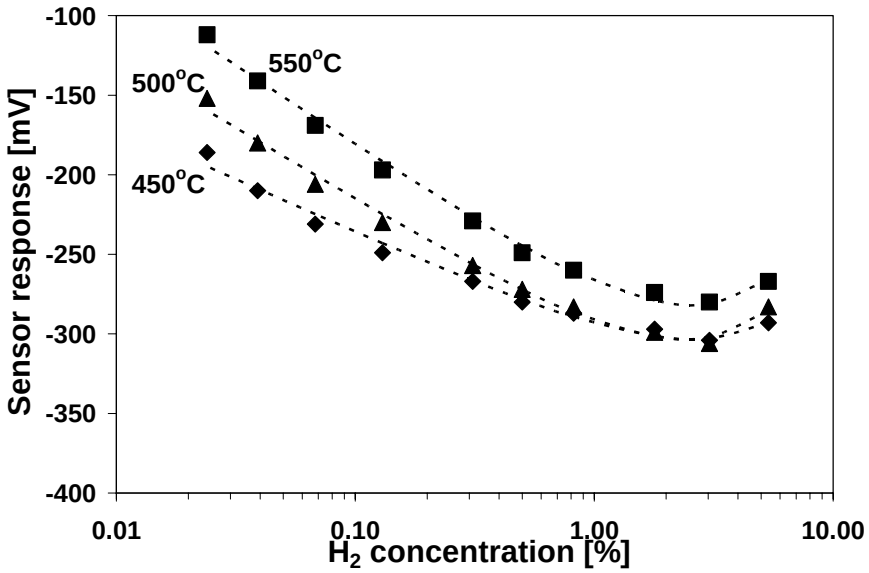

Fig 4: Sensor response (13 μm sensing electrode) versus H_2 concentration at 450, 500 and 550°C. The dotted lines show the best fit of Eq. (7) to the data.

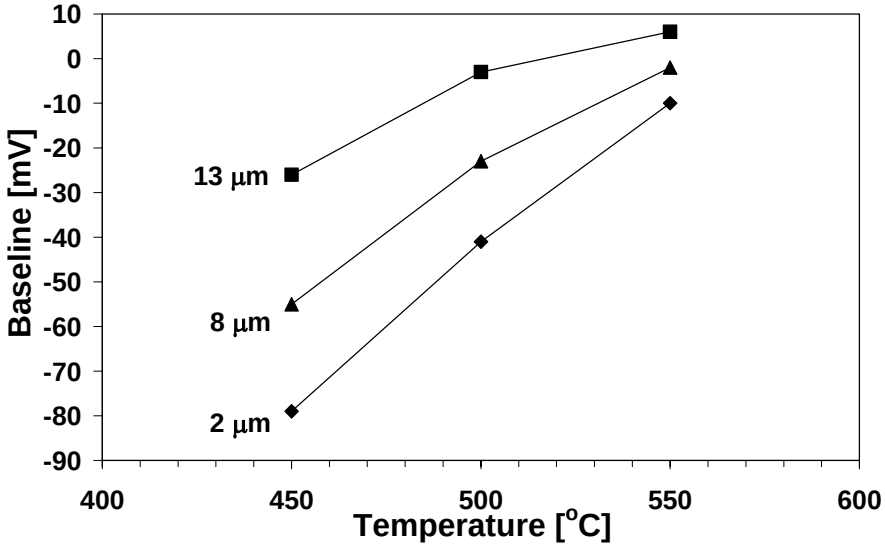

Figure 5: Baselines in ambient air versus operating temperature for aged sensors with sensing electrode thicknesses of 2, 8, and 13 μm.

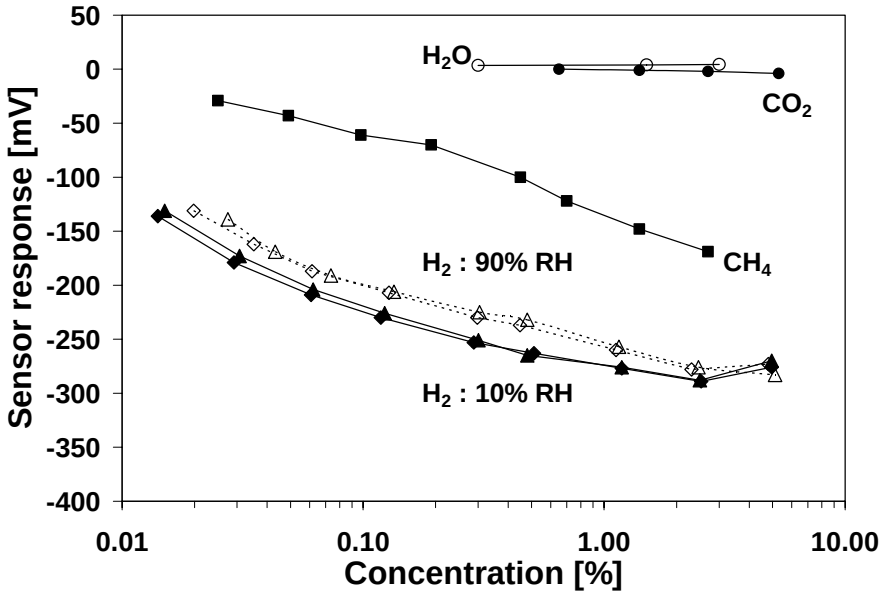

Figure 6: Response at 500°C of an aged sensor (13 μm sensing electrode) to H_2 in 10% (♦, ▲) and 90% (◊, Δ) relative humidity (RH). The two curves at each humidity level represent before and after 18 hrs at 90% relative humidity (see text). Also shown, response to CH_4, CO_2, and H_2O.

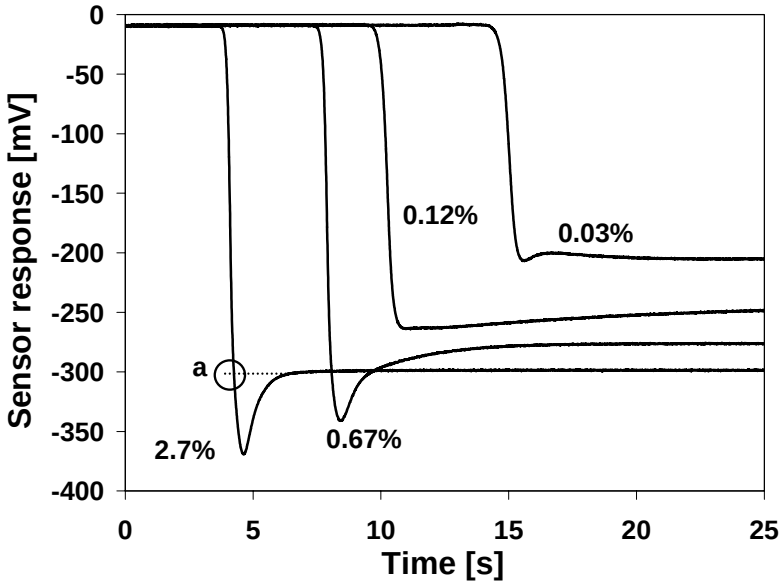

Figure 7a: Sensor response at 500^{o}C versus time for 2.7, 0.67, 0.12 and 0.03% H_2.

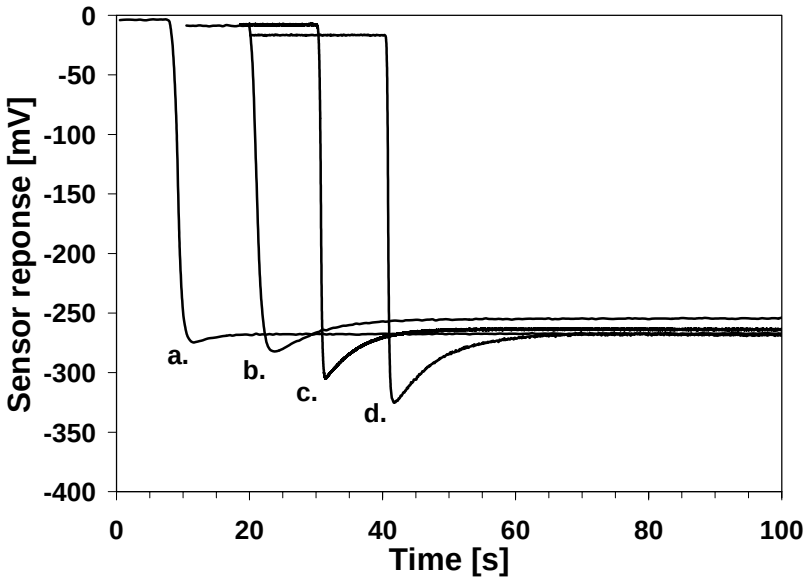

Figure 7b: Evolution of the transient overshoot in the sensor response to 0.5% H_2 after operation at 500^{o}C for: a) 86 hrs, b) 117 hrs, c) 124 hrs, and d) 148 hrs.

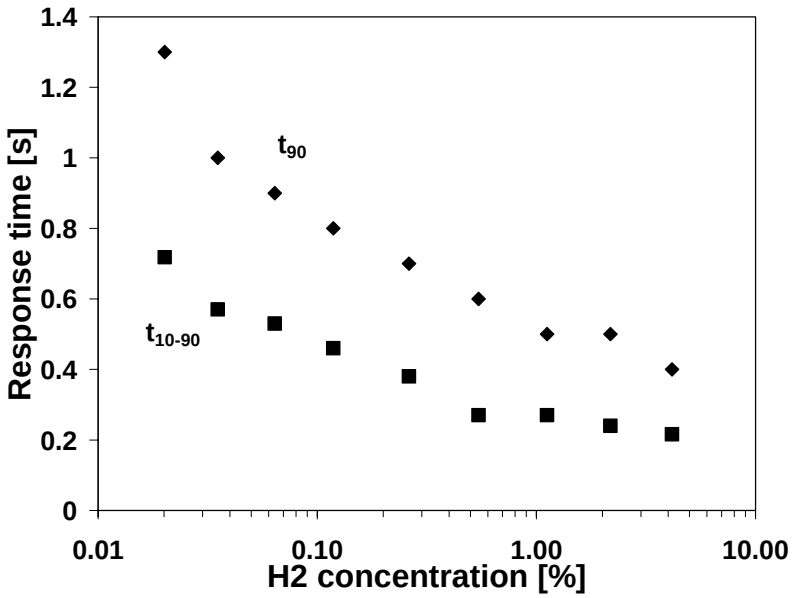

Figure 8: Sensor response time as a function of H_2 concentration. Response times are measured from the baseline to 90% of the full response (t_{90}) and from 10% to 90% of the full response ($t_{10\text{-}90}$).

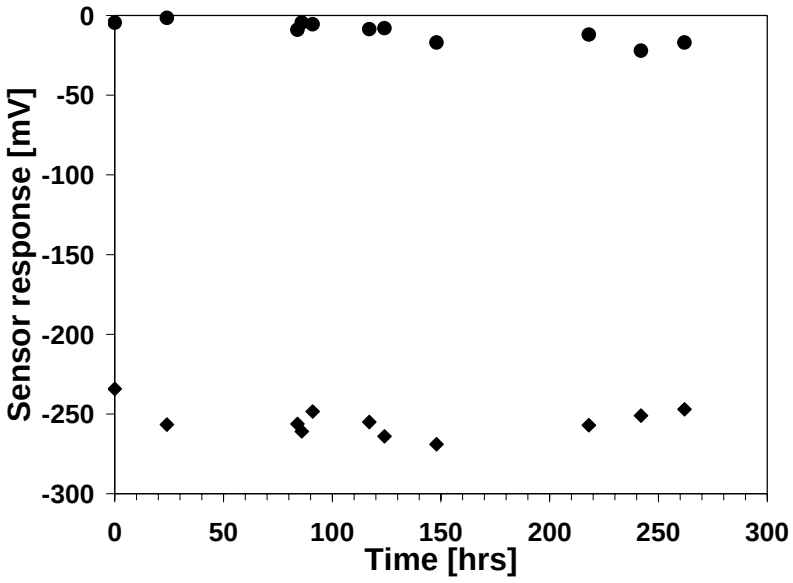

Figure 9: Sensor baseline (●) and response to 0.3% H_2 (♦) as a function of time at 500°C.